Quantitative analysis of the physiological contributions of glucose to the TCA cycle

Shiyu Liu[1,2] , Ziwei Dai[2], Daniel E. Cooper[3], David G. Kirsch[2,3] and Jason W. Locasale[4]*

[1]Computational Biology and Bioinformatics Program, Duke Center for Genomics and Computational Biology, Duke University School of Medicine, Durham NC 27710, USA

[2]Department of Pharmacology and Cancer Biology, Duke University School of Medicine, Durham NC 27710, USA

[3]Department of Radiation Oncology, Duke University Medical Center, Durham NC 27710, USA

[4]Morrisville NC 27560, USA

*Correspondence to Jason W. Locasale – dr.jason.locasale@gmail.com

ABSTRACT

The carbon source for catabolism *in vivo* is a fundamental question in metabolic physiology. Limited by data and rigorous mathematical analysis, many controversial statements exist on the metabolic sources for carbon usage in the tricarboxylic acid (TCA) cycle under physiological settings. Using isotope-labeling data *in vivo* across several experimental conditions, we construct multiple models of central carbon metabolism and develop methods based on metabolic flux analysis (MFA) to solve for the preferences of glucose, lactate, and other nutrients used in the TCA cycle across many tissues. We show that in nearly all circumstances, glucose contributes more than lactate as a nutrient source for the TCA cycle. This conclusion is verified in different animal strains, different administrations of 13C glucose, and is extended to multiple tissue types after considering multiple nutrient sources. Thus, this quantitative analysis of organismal metabolism defines the relative contributions of nutrient fluxes in physiology, provides a resource for analysis of *in vivo* isotope tracing data, and concludes that glucose is the major nutrient used for catabolism in mammals.

INTRODUCTION

Cellular metabolism that resides within tissues utilizes many metabolites as their source in the TCA cycle such as glucose, lactate, amino acids, and fatty acids. As part of systemic metabolism, each cell

has unique preferences for the utilization of particular metabolites, which is influenced by tissue type, cell state, environmental factors such as nutrition and physiological status. The nutrient preferences are not only critical for normal organ function, but also closely linked to disease. For example, the fermentative glucose metabolism known as the Warburg effect has been widely found in numerous types of healthy and malignant cells (Liberti and Locasale, 2016), but glucose utilization is highly variable and depends on genetics and environment (Faubert et al., 2017; Feron, 2009; Hensley et al., 2016). Those specific metabolic fluxes could be potential targets for cancer treatment (Liberti et al., 2017; Sonveaux et al., 2008). For other tissues like the myocardium, the energy contribution from fatty acids, glucose, lactate and others are thought to directly reflect its nutrient and oxygen availability, and have important roles in heart failure (Crawford et al., 2009; Kodde et al., 2007). Therefore, investigation for nutrient source utilization in physiological conditions is of utmost importance.

To distinguish and quantitate different nutrient sources, isotope-labeling-based methods have long been used. Cells or animals are fed or infused with isotopically-labeled substrates, and labeling ratios of metabolites are analyzed by mass spectrometry (MS) or nuclear magnetic resonance (NMR). Previous studies have used these data to qualitatively explain the contribution of nutrients sources to the TCA cycle (Stanley et al., 1988). However, those studies have been limited by measurements that often included only a few metabolites. Recent studies have looked to quantitatively measure the utilization of nutrient sources at the systemic level using metabolic flux analysis (MFA) (Hui et al., 2017; Jang et al., 2019; Neinast et al., 2019). MFA is a methodology that seeks a solution of metabolic fluxes that best fits the isotope labeling data (i.e. machine learning or artificial intelligence) for a given biochemical reaction network (Dai and Locasale, 2017; Zamboni et al., 2009). The biochemical model used is essential for the resulting solutions. For instance, reversible (i.e. exchange) fluxes of metabolites between tissue and plasma are almost always significant and may highly influence isotope labeling patterns (Witney et al., 2011). However, many MFA models do not consider exchange fluxes (Hui et al., 2017). Another important point is the heterogeneity of metabolism. Some researchers have shown that metabolic heterogeneity exists widely in within and between lung cancers (Hensley et al., 2016). Organismal metabolism relies on mutual cooperation between tens of organs and tissues. However, most current MFA models only focus on flux calculation in one kind of tissue and regard the tissue as a homogenous system.

To investigate the quantitative selection of nutrient sources of entry into the TCA cycle under physiological conditions, we developed a framework to overcome current challenges. Multiple tissues are considered, linked by circulation. This model also uses the MFA method and requires isotope-labeling data for different tissues to fit fluxes in different compartments. Surprisingly we found that under physiological conditions, as we validated using different animal models and experimental isotope labeling conditions, most tissues utilize circulating glucose more than lactate for the TCA cycle which challenges current dogma in metabolic physiology.

RESULTS

Model construction and flux analysis

In the fasting state, systemic metabolism involves a source tissue (usually liver) that converts circulating lactate to glucose in blood, and a sink tissue that consumes glucose back to lactate, which is referred as the Cori cycle (Nelson et al., 2017) (Figure 1A). Glucose and lactate in the source and sink tissues are interconverted through pyruvate. Sink and source tissues are connected through plasma, which allows for the free diffusion of glucose and lactate (Figure 1B).

Fluxes are computed based on data from mass spectrometry (MS) in the ^{13}C-glucose infused mouse as follows. After infusion, tissues are collected and analyzed by MS. Metabolites with different numbers of ^{13}C are distinguished and their relative abundance is referred to as the metabolite isotopomer distribution (MID) (Figure 1C). MID data are used to fit the fluxes in the model. Given a set of fluxes, MIDs can be predicted and compared with experimental data. Differences between prediction and experiments, measured by the Kullback-Leibler divergence (Kullback and Leibler, 1951), are used as a cost function. After sampling the solution space, all flux sets with a sufficiently low cost function value are considered as valid solutions (Figures 1D, E, S1A, S1B, supplementary methods).

Glucose contributions in different tissues

The flux network can be mathematically defined with a simplified diagram: the TCA cycle in the source and sink tissue is fed by two fluxes from glucose and lactate in plasma (Figure 2A, supplementary methods). Non-negative contribution fluxes to TCA cycle from glucose (F_{glc} in source tissue and G_{glc} in sink tissue) or from lactate (F_{lac} in source tissue and G_{lac} in sink tissue) are calculated from net fluxes of related reactions and diffusion (supplementary methods). From the computed fluxes, the glucose

contribution ratio R_{glc} is calculated to reflect the relative ratio of glucose contribution to the TCA cycle. If R_{glc} is higher than 0.5, it implies that glucose contributes more than lactate to TCA cycle. If it is lower than 0.5, lactate contributes more than glucose (Figure 2B).

To evaluate the glucose contribution, feasible solutions are sampled from the solution space and displayed in a violin plot (Figure 2C). The source tissue is the liver and the sink tissues are set as heart, brain, skeletal muscle, kidney, lung, pancreas, small intestine and spleen. Median levels of glucose contribution for all sink tissue are higher or close to 0.5 (Figure 2D, S1C). Therefore, in most tissues, glucose contributes more than lactate to the TCA cycle.

The results from these two-tissue models rely on MID data and some parameters. To evaluate these dependencies, we implemented a Monte Carlo based sensitivity analysis (Shestov et al., 2014). First, original data and parameters are perturbed randomly. The perturbed values are used to calculate distribution of R_{glc} as previously described. After this process, the median of this distribution under each individual perturbation is collected, and the distribution of median R_{glc} reflects its sensitivity to data and parameters (Figure S2A). Results show that under all perturbations of flux parameters, the median R_{glc} is always higher than 0.5 (Figure S2B, C, D). In most perturbations to the MID data, the median R_{glc} is also higher than 0.5 (Figure S2E). These results demonstrate the robustness of the conclusion that glucose contributes more than lactate to the TCA cycle under physiological conditions.

Generality of the glucose contribution to the TCA cycle

To further investigate the generality of this conclusion, we considered a different animal strain, different diet and different infusion protocol with mice infused with ^{13}C-glucose at a higher infusion rate which is one of the key technical variables of consideration in these studies (Ayala et al., 2010). In addition to our analysis of published data (Hui et al., 2017), these new experiments expand the scope of physiological variables (Figure 3A). These data are referred to as “high-infusion rate”, while the previous analysis is referred to as “low-infusion rate”. Because of the higher infusion rate, an input flux J_{in} in plasma is added to the model to capture the infusion operation (Figure 3B). The amount of ^{13}C labeling increases with the infusion rate, and with a higher infusion rate, the value of the cost function reaches a lower value indicating a better fit of the data (Figure S3A, S3B). As defined previously, the glucose

contribution R_{glc} to the TCA cycle is calculated (Figure 3C). The analysis shows that in most cases, R_{glc} is higher than 0.5, again implying that glucose contributes more than lactate to the TCA cycle (Figure 3D, S3C).

Glucose contribution upon consideration of multiple tissue interactions

The current model is based on source and sink tissues. However, mammals consist of tens of different tissues which cooperate and interact. To demonstrate the utility of this model to multiple tissue compartments, more sink tissues are introduced and the glucose contribution under these conditions are analyzed. This model contains one source tissue and two sink tissues, which are connected by glucose and lactate in plasma (Figure 4A, B). This model fits well with low-infusion data with the threshold of objective value (Figure S4A, S4B). In this model, glucose and lactate in plasma can contribute to the TCA cycle through three kinds of tissue, and therefore the definition of glucose contribution is slightly modified (Figure 4C). In this multi-tissue model, glucose contributes more than lactate to the TCA cycle (Figure 4D).

Glucose contribution upon consideration of multiple nutrient sources

The current analysis considers two circulating metabolites as sources for the TCA cycle: glucose and lactate. However, many other metabolites circulate and are exchanged between tissue and plasma, such as acetate, alanine and pyruvate (Hui et al., 2017; Liu et al., 2018). Therefore, to investigate the applicability of this model, circulating pyruvate is introduced (Figure 5A). Circulating pyruvate can also represent other nutrient sources including but not limited to alanine, glutamine, acetate, or fatty acids. In this model, circulating pyruvate is not only exchanged with sink and source tissue, but also converted to lactate in plasma. Glucose and lactate in plasma can also be directly converted to pyruvate (Figure 5B). This model converges well with both low-infusion rate and high-infusion rate data with different thresholds of objective value (Figure S5A, S5B, S6A). Because circulating glucose, lactate and pyruvate each contributes to the TCA cycle in source and sink tissues, the contribution ratios of the three metabolites R_{glc}, R_{lac} and R_{pyr} need to be calculated individually, and the sum of the three contribution ratios equals to 1 (Figure 5C). The distribution of three ratios can be displayed by a ternary plot (Marc et al., 2019, supplementary methods). For the low-infusion rate data, the contribution from

glucose is slightly higher than lactate, and much higher than pyruvate (Figure 5D). The conclusion is similar when the sink tissue in the model is replaced by other types of tissue (Figure S6B). For the high-infusion rate data, the contribution from glucose markedly dominates in all sampled solutions (Figure 5E). Therefore, in situations with more nutrient sources, glucose still contributes more than lactate to the TCA cycle.

DISCUSSION

The nutrient sources for the TCA cycle have long been of interest. However, due to difficulties in data acquisition and mathematical analysis, quantitative studies under physiological conditions are still rare. With advances in mass spectrometry and mathematical modeling, *in vivo* flux analysis studies with isotope-labeling data have become a mainstay in the study of metabolic physiology. Previous studies have measured TCA cycle source utilization by MFA. However, with the development of these new mathematical tools, our study challenges some key conclusions that form the current consensus for the relative contributions of lactate and glucose to the TCA cycle. For example, it was reported that lactate is the major energy source for most tissues and tumors (Hui et al., 2017; Jin et al., 2019). Our results show that most organs uptake more glucose than lactate to fuel the TCA cycle. This conclusion also holds under various parameters, experimental conditions such as animal strain and diet, tissue type, tissue interactions and source metabolite number, which together indicate the robustness and generalizability of the conclusions. Our results, however, are consistent with conventional knowledge that glucose behaves as a primary energy source in cells and tissues, especially for neural systems (Nelson et al., 2017). Nevertheless, our results confirm that lactate is highly exchanged between tissue and plasma, while glucose is transferred from the liver to other organs. These phenomena appear to also be observed in recent studies on flux measurements in pigs (Jang et al., 2019).

Another intriguing feature of this model is its generalizability and scalability. From a basic two-tissue version, this model is readily extended to compute fluxes from isotope patterns with higher infusion rates, more tissue types and more nutrient sources which could be useful to study for example different nutritional situations and pathophysiology states such as metabolic syndromes, diabetes and cardiovascular disease. The generality of this model allows for a broader usage in future research. More kinds of tissue can be introduced to better mimic the physiological condition such as the interaction between cancer and host organs. As the number of tissues increases, their roles could be more complicated rather than simple source and sink. For example, previous research indicates that the

kidney may also have a significant contribution to net production of glucose in pigs (Jang et al., 2019). Second, more nutrient sources could be introduced and the metabolic network in each cell could also be expanded. The current model includes three nodes: glucose, pyruvate and lactate which capture fluxes in central carbon metabolism but could be extended into intermediary metabolism. Although sufficient for analyzing the contribution of macronutrients, studies of fatty acids, ketosis and amino acid metabolism will require a larger network. Nevertheless, the methodology contained within this model could be extended. For instance, subcellular compartmentalized metabolic flux analysis is also important (Lee et al., 2019). However, its application is usually restricted to the mitochondria and nucleus because of the difficulty in acquiring isotope-labeling data in each cellular compartment. On the other hand, interactions within heterogenous tissues could also be described by this model. It has been widely shown that cells in a tumor may express different metabolic states, and will compete or cooperate for many resources (Hensley et al., 2016). Quantitative methods based on this model may help to better describe those precise and complicated interactions.

Our ability to resolve metabolic fluxes is limited by the availability of high-quality data. Thus, limited by data and computational resources, this model only covers a small portion of biochemical reactions. However, in the condition with three tissues and three energy sources, high dimensionality of tge solution space requires that the sampling procedures used become important to correctly assess the uncertainty in the flux calculations. As the model expands, the solution space might be too high dimensional to sample efficiently. Thus, more constraints must be introduced to reduce the dimensionality of the feasible solution space. For example, our study includes constraints from circulatory fluxes (Hui et al., 2017), and some MFA model uses fixed biomass fluxes as boundary conditions (Reid et al., 2018). However, the precision and generalizability of these external constraints have not been rigorously validated, and they may introduce bias. Comprehensive and precise model analysis requires more effort to establish reliable constraints as well as acquisition of metabolite data with more coverage and higher resolution.

METHODS

Data Sources

This study is based on two data sources: low-infusion data were obtained from infused fasting mice in previous work (Hui et al., 2017), while the high-infusion data were acquired based on following protocols.

Reagents

Unless otherwise specified, all reagents were purchased from Sigma-Aldrich. Jugular vein catheters, vascular access buttons, and infusion equipment were purchased from Instech Laboratories. Stable isotope glucose were purchased from Cambridge Isotope Laboratories.

Animal Models

All animal procedures were approved by the Institutional Animal Care and Use Committee (IACUC) at Duke University. Mouse models is from 8 to 10-week old, male and female mixed background (129/SVJae and C57BL/6) with a combination of alleles that have been previously described: $Pax7^{CreER\text{-}T2}$, $p53^{FL/FL}$, LSL-$Nras^{G12D}$ and $ROSA26^{mTmG}$ (Zhang et al., 2015). Mice were fed standard laboratory chow diets *ad libitum*.

***In vivo* ^{13}C glucose infusions**

To perform in vivo nutrient infusions, chronic indwelling catheters were placed into the right jugular veins of mice and animals were allowed to recover for 3-4 days prior to infusions. Mice were fasted for 6 hours and infused with [U-13C]glucose for 3 hours at a rate of 20 mg/kg/min (150 µL/hr). Blood was collected via the tail vein at 3 h and serum was collected by centrifuging blood at 3000g for 15 min at 4°C. At the end of infusions, tissues were snap frozen in liquid nitrogen and stored at -80°C for further analyses.

Metabolite extraction from tissue

Briefly, the tissue sample was first homogenized in liquid nitrogen and then 5 to 10 mg was weighed in a new Eppendorf tube. Ice cold extraction solvent (250 µl) was added to tissue sample, and a pellet mixer was used to further break down the tissue chunk and form an even suspension, followed by addition of 250 µl to rinse the pellet mixer. After incubation on ice for an additional 10 min, the tissue extract was centrifuged at a speed of 20 000 g at 4 °C for 10 min. 5 µl of the supernatant was saved in -80 °C freezer until ready for further derivatization, and the rest of the supernatant was transferred to a new Eppendorf tube and dried in a speed vacuum concentrator. The dry pellets were reconstituted into 30 µl (per 3 mg tissue) sample solvent (water:methanol:acetonitrile, 2:1:1, v/v) and 3 µl was injected to LC-HRMS.

HPLC method

Ultimate 3000 UHPLC (Dionex) was used for metabolite separation and detection. For polar metabolite analysis, a hydrophilic interaction chromatography method (HILIC) with an Xbridge amide column (100 x 2.1 mm i.d., 3.5 µm; Waters) was used for compound separation at room temperature. The mobile phase and gradient information were described previously. 2-hydrazinoquinoline derivatives were measured using reversed phase LC method, which employed an Acclaim RSLC 120 C8 reversed phase column (150 x 2.1 mm i.d., 2.2 µm; Dionex) with mobile phase A: water with 0.5% formic acid, and mobile phase B: acetonitrile. Linear gradient was: 0 min, 2% B; 3 min, 2% B; 8 min, 85% B;9.5 min, 98% B; 10.8 min, 98% B, and 11 min, 2% B. Flow rate: 0.2 ml/min. Column temperature: 25 °C.

Mass Spectrometry

The Q Exactive Plus mass spectrometer (HRMS) was equipped with a HESI probe, and the relevant parameters were as listed: heater temperature, 120 °C; sheath gas, 30; auxiliary gas, 10; sweep gas, 3; spray voltage, 3.6 kV for positive mode and 2.5 kV for negative mode. Capillary temperature was set at 320°C, and S-lens was 55. A full scan range was set at 70 to 900 (*m/z*) with positive/negative switching when coupled with the HILIC method, or 170 to 800 (*m/z*) at positive mode when coupled with reversed phase LC method. The resolution was set at 140 000 (at *m/z* 200). The maximum injection time (max IT) was 200 ms at resolution of 70 000 and 450 ms at resolution of 140 000. Automated gain control (AGC) was targeted at 3 × 106 ions. For targeted MS2 analysis, the isolation width of the precursor ion was set at 1.0 (*m/z*), high energy collision dissociation (HCD) was 35%, and max IT is 100 ms. The resolution and AGC were 35 000 and 200 000, respectively.

Metabolite Peak Extraction and Data Analysis

Raw peak data was processed on Sieve 2.0 software (Thermo Scientific) with peak alignment and detection performed according to the manufacturer's protocol. The method "peak alignment and frame extraction" was applied for targeted metabolite analysis. An input file of theoretical *m/z* and detected retention time was used for targeted metabolite analysis, and the *m/z* width was set to 5 ppm. An output file was obtained after data processing that included detected *m/z* and relative intensity in the different samples.

Metabolic flux analysis

Flux model and constraints

The flux model includes biochemical reactions and diffusions between tissue and plasma. The model covers glucose, lactate and pyruvate in two or three kinds of tissue and plasma (figure 1(b)). All metabolites were assumed to be balanced during simulations, which means sum of income fluxes to a certain metabolite equals to sum of outgo fluxes from this metabolite. Circulatory flux constraints were implemented to reduce degrees of freedom (Hui et al., 2017).

MID prediction, flux fitting and solution sampling

An iterative optimization algorithm was used to compute the fluxes. Given a set of flux values, MID of target metabolites can be predicted from averaging MID of precursors using flux values as weights:

$$\tilde{\boldsymbol{M}}_i = \frac{\sum_j F_j \boldsymbol{M}_{ji}}{\sum_j F_j} \tag{S1}$$

where $\tilde{\boldsymbol{M}}_i$ is the predicted MID of metabolite i, $\boldsymbol{M}_{ji}$ is MID of metabolite i produced from its precursor metabolite j, and F_j is the flux from j to i.

The difference between the predicted and experimental MIDs was evaluated by Kullback–Leibler divergence:

$$L_i = \boldsymbol{M}_i \log \frac{\tilde{\boldsymbol{M}}_i}{\boldsymbol{M}_i} \tag{S2}$$

where $\tilde{\boldsymbol{M}}_i$ is predicted MID and $\boldsymbol{M}_i$ is experimental MID of metabolite i. Sum of L_i for all target metabolites was regarded as the cost function to minimize. The optimization problem was defined as:

$$\min_{\boldsymbol{F}} L_{model}(\boldsymbol{F}), \text{ s.t. } \boldsymbol{A}\cdot\boldsymbol{F} = \boldsymbol{b} \text{ and } F_{\min} \le \boldsymbol{F} \le F_{\max} \tag{S3}$$

where $\boldsymbol{F}$ is the vector of all fluxes and $\boldsymbol{A}\cdot\boldsymbol{F} = \boldsymbol{b}$ represents flux balance requirement and other constraints.

To better cover all possible results, the high-dimensional solution space was sampled and all solutions with cost function value lower than a threshold were selected for further calculations.

Glucose contribution calculation

After fitting a flux from MID data, glucose contribution was calculated to quantify the net contribution from glucose in plasma to TCA cycle. First, the contribution flux from each circulating metabolite was calculated. The contribution flux was calculated by the net flux from the plasma to each kind of tissue,

minus the part which flows out of the tissue in the form of other metabolites (see supplementary methods for details). Then, the contribution flux was normalized to total contribution flux from all carbon sources to calculate the relative contribution ratio.

All valid flux solutions were analyzed for glucose contribution, and their relative ratios were displayed on the violin plot.

Parameter sensitivity analysis

Experimental MID data or flux constraints were perturbed by multiplying Gaussian-distributed noises. After each perturbation, the perturbed value was used to solve fluxes and calculate distribution of glucose contribution. Then the median value of the distribution was calculated. Median values from all perturbations were collected and displayed by violin plot.

Ternary graph plotting

Contributions from three energy sources were visualized by ternary graph. All triplets of contribution ratios were plotted on the triangle and density of distribution was rendered by a Gaussian kernel. In the rendering process, convolutions between all points and Gaussian distribution were calculated, and the resulting density was converted into space of ternary graph to be displayed.

Software implementation

Scripts in this study were implemented by Python 3.6. Source codes are available from GitHub (https://github.com/LocasaleLab/Lactate_MFA). The package version dependency is also provided on GitHub website. A Docker on Linux system for out-of-the-box running is also available. Each model requires around 10 ~ 50 hours of running time.

ACKNOWLEDGEMENTS

We thank members of the Locasale laboratory for helpful discussions. Support from National Institutes of Health (R01CA193256, R35CA197616) and the American Cancer Society (RSG-16-214-01-TBE) are gratefully acknowledged.

AUTHOR CONTRIBUTIONS

S.L., Z.D., and J.W.L. designed the study. S.L. and J.W.L. wrote the manuscript with essential input from Z.D. S.L. developed the model and performed the data analysis with help from Z.D. D.E.C. performed *in*

vivo nutrient infusions and reviewed results with D.G.K. All authors have read, edited and approved the final manuscript.

LEGENDS

Figure 1. General methodology and flux analysis. (a) Diagram of metabolite exchange between source and sink tissues. Glycogen, amino acids and other nutrition source are utilized to supplement glucose in the source tissue. (b) Three components (source tissue, plasma and sink tissue) and two circulating metabolites (lactate and glucose). (c) Data acquisition. Tissues of ^{13}C-infused mice are extracted and analyzed by mass spectrometry. Distribution of mass isotopomers for metabolites, such as glucose, lactate and pyruvate, are used to solve for the fluxes (b). Definition of cost function. (e) Schematic and example of a feasible solution.

Figure 2. Contribution to the TCA cycle from circulating glucose. (a) Diagram of contribution fluxes. Glucose and lactate can contribute to TCA by F_{glc} and F_{lac} in the source tissue, while G_{glc} and G_{lac} are related to the sink tissue. (b) Definition of glucose contribution ratio based on fluxes in (a). R_{glc} is a scalar between 0 and 1. Higher R_{glc} represents an increasing glucose contribution to the TCA cycle. (c) Procedure to compute distribution of glucose contribution. Feasible solutions are sampled and glucose contribution ratios are calculated. The distribution of glucose contribution is displayed by a violin plot. (d) Distribution of glucose contribution based on a model with different sink tissues. For all sink tissues, the median of glucose contribution is close to or higher than 0.5, which means glucose contributes more than lactate to the TCA cycle.

Figure 3. Robustness of results relative to animal model and infusion rate. (a) A higher infusion rate and longer infusion time, which leads to higher abundance of ^{13}C in most metabolites. The genetic background and diet are also different from previous experiments. (b) Structure of high-infusion model. The main difference is ^{13}C labeled infusion to glucose in plasma. (c) Definition of glucose contribution. Glucose and lactate in plasma contribute to the TCA cycle in the source and sink tissue. (d) Distribution of glucose contribution shows glucose contributes more than lactate to the TCA cycle. The source tissue is liver and sink tissue is skeletal muscle.

Figure 4. Flux analysis across multiple tissues. (a) A model with additional sink tissues. (b) Structure of the multi-tissue model. One source tissue and two sink tissues are connected by glucose and lactate in the plasma. (c) Contribution of metabolites is defined. Glucose and lactate can contribute to TCA by F_{glc} and F_{lac} in the source tissue, G_{glc} and G_{lac} in the sink tissue 1, and H_{glc} and H_{lac} in sink tissue 2, respectively. The glucose contribution is defined as the relative ratio of glucose contribution flux among all tissues. (d) Distribution of glucose contribution shows glucose contributes more than lactate to the TCA cycle. The source tissue is liver and sink tissues are heart and skeletal muscle. The low-infusion rate data is used to solve this model.

Figure 5. Robustness of results to multiple circulating metabolites feeding the TCA cycle. (a) Incorporation of additional circulating metabolites. (b) The structure of the model. The source tissue and sink tissue are connected with glucose, lactate and pyruvate in the plasma. (c) Contribution from metabolites is defined. Glucose, lactate and pyruvate can contribute to the TCA cycle by F_{glc}, F_{lac} and F_{pyr} in source tissue, and G_{glc}, G_{lac} and G_{pyr} in the sink tissue. The glucose contribution is defined by the relative ratio of the glucose contribution flux to that of the other metabolites. (d) Ternary plot to display distribution of contributions from three metabolites. The orange point indicates average level. (e) Analysis and results as in (d) but for additional high-infusion system of different animal strain, different diet and different infusion protocol. The source tissue is liver and sink tissue is skeletal muscle.

Figure S1. Detailed information of model fitting. (a) Example of predicted and experimental MID in the model with threshold objective value. Value of objective function is 0.1. Experimental MID could be well fitted by this model. (b) Distribution of objective function for two free fluxes. (c) Distribution of glucose contribution for two free fluxes. For all subplots in (b) and (c), the source tissue is liver, while the sink tissue is as labeled. See supplementary methods for details of free fluxes.

Figure S2. Parameter sensitivity analysis. (a) Original MID data or constraint parameters are randomly perturbed and used in the following analysis. The resulting distribution of the glucose contribution for each perturbation is calculated, and their medians are collected. Distribution of medians reflects parameter sensitivities for this model. The distribution of medians under perturbation of glucose circulatory flux (b), lactate circulatory flux (c), input flux in source tissue (d) and MID data (e). Most of

the medians are above the 0.5 threshold, which implies that under most perturbations, glucose contributes more than lactate to the TCA cycle. (f) Distribution of medians of the objective value under those perturbations. The threshold line for feasible solutions is displayed with an orange dash.

Figure S3. Detailed information for the high-infusion system. (a) Example of predicted and experimental MID in the high-infusion model with threshold objective value. The value of the objective function is 0.25. For this threshold, the experimental MID could be predicted in the high-infusion system. Notably, the ratio of high ^{13}C isotopomer is significantly higher than that of the original system. (b) Distribution of objective function for two free fluxes. (c) Distribution of glucose contribution for two free fluxes. In fitting the high-infusion system, the source tissue is liver and sink tissue is skeletal muscle. See supplementary methods for details of the free fluxes.

Figure S4. Detailed information of the multi-tissue model. (a) Example of predicted and experimental MID in the multi-tissue model with a threshold objective value of 0.15. For this threshold, the experimental MID could be predicted by the high-infusion model. (b) Distribution of objective function value. Objective values are mostly below the threshold.

Figure S5. (a) Example of predicted and experimental MID for model with multiple circulating metabolites. The model is fitted with low-infusion data. (b) same as in (a) but fitted with high-infusion data. Their threshold objective values are 0.15 and 0.25 respectively.

Figure S6. (a) Contributions to the TCA cycle when additional nutrients are considered. Subplots have a common source tissue (i.e. liver) but different sink tissues. For most sink tissues, glucose contributes to the TCA cycle more than lactate and pyruvate, especially in heart, brain, kidney and small intestine. The orange point indicates average level. (b) Distribution of objective values obtained from fitting with different data sets. The dashed orange line denotes the threshold objective value.

REFERENCES

Ayala, J.E., Samuel, V.T., Morton, G.J., Obici, S., Croniger, C.M., Shulman, G.I., Wasserman, D.H., McGuinness, O.P., and Consortium, N.I.H.M.M.P.C. (2010). Standard operating procedures for describing and performing metabolic tests of glucose homeostasis in mice. Dis Model Mech *3*, 525-534.

Crawford, P.A., Crowley, J.R., Sambandam, N., Muegge, B.D., Costello, E.K., Hamady, M., Knight, R., and Gordon, J.I. (2009). Regulation of myocardial ketone body metabolism by the gut microbiota during nutrient deprivation. Proceedings of the National Academy of Sciences *106*, 11276-11281.

Dai, Z., and Locasale, J.W. (2017). Understanding metabolism with flux analysis: From theory to application. Metabolic Engineering *43*, 94-102.

Faubert, B., Li, K.Y., Cai, L., Hensley, C.T., Kim, J., Zacharias, L.G., Yang, C., Do, Q.N., Doucette, S., Burguete, D.*, et al.* (2017). Lactate Metabolism in Human Lung Tumors. Cell *171*, 358-371.e359.

Feron, O. (2009). Pyruvate into lactate and back: from the Warburg effect to symbiotic energy fuel exchange in cancer cells. Radiotherapy and oncology *92*, 329-333.

Hensley, Christopher T., Faubert, B., Yuan, Q., Lev-Cohain, N., Jin, E., Kim, J., Jiang, L., Ko, B., Skelton, R., Loudat, L.*, et al.* (2016). Metabolic Heterogeneity in Human Lung Tumors. Cell *164*, 681-694.

Hui, S., Ghergurovich, J.M., Morscher, R.J., Jang, C., Teng, X., Lu, W., Esparza, L.A., Reya, T., Le, Z., Yanxiang Guo, J.*, et al.* (2017). Glucose feeds the TCA cycle via circulating lactate. Nature *551*, 115-118.

Jang, C., Hui, S., Zeng, X., Cowan, A.J., Wang, L., Chen, L., Morscher, R.J., Reyes, J., Frezza, C., Hwang, H.Y.*, et al.* (2019). Metabolite Exchange between Mammalian Organs Quantified in Pigs. Cell Metabolism.

Jin, N., Bi, A., Lan, X., Xu, J., Wang, X., Liu, Y., Wang, T., Tang, S., Zeng, H., Chen, Z.*, et al.* (2019). Identification of metabolic vulnerabilities of receptor tyrosine kinases-driven cancer. Nature Communications *10*, 2701.

Kodde, I.F., van der Stok, J., Smolenski, R.T., and de Jong, J.W. (2007). Metabolic and genetic regulation of cardiac energy substrate preference. Comp Biochem Physiol A Mol Integr Physiol *146*, 26-39.

Kullback, S., and Leibler, R.A. (1951). On information and sufficiency. The annals of mathematical statistics *22*, 79-86.

Lee, W.D., Mukha, D., Aizenshtein, E., and Shlomi, T. (2019). Spatial-fluxomics provides a subcellular-compartmentalized view of reductive glutamine metabolism in cancer cells. Nature Communications *10*, 1351.

Liberti, M.V., Dai, Z., Wardell, S.E., Baccile, J.A., Liu, X., Gao, X., Baldi, R., Mehrmohamadi, M., Johnson, M.O., Madhukar, N.S.*, et al.* (2017). A Predictive Model for Selective Targeting of the Warburg Effect through GAPDH Inhibition with a Natural Product. Cell Metabolism *26*, 648-659.e648.

Liberti, M.V., and Locasale, J.W. (2016). The Warburg Effect: How Does it Benefit Cancer Cells? Trends in Biochemical Sciences *41*, 211-218.

Liu, X., Cooper, D.E., Cluntun, A.A., Warmoes, M.O., Zhao, S., Reid, M.A., Liu, J., Lund, P.J., Lopes, M., Garcia, B.A., *et al.* (2018). Acetate Production from Glucose and Coupling to Mitochondrial Metabolism in Mammals. Cell *175*, 502-513.e513.

Marc, Weinstein, B., tgwoodcock, Simon, C., chebee7i, Morgan, W., Knight, V., Swanson-Hysell, N., Evans, M., jl-bernal, *et al.* (2019). marcharper/python-ternary.

Neinast, M.D., Jang, C., Hui, S., Murashige, D.S., Chu, Q., Morscher, R.J., Li, X., Zhan, L., White, E., and Anthony, T.G. (2019). Quantitative analysis of the whole-body metabolic fate of branched-chain amino acids. Cell metabolism *29*, 417-429. e414.

Nelson, D.L., Cox, M.M., and Lehninger, A.L. (2017). Lehninger principles of biochemistry.

Reid, M.A., Allen, A.E., Liu, S., Liberti, M.V., Liu, P., Liu, X., Dai, Z., Gao, X., Wang, Q., Liu, Y., *et al.* (2018). Serine synthesis through PHGDH coordinates nucleotide levels by maintaining central carbon metabolism. Nature Communications *9*, 5442.

Shestov, A.A., Liu, X.J., Ser, Z., Cluntun, A.A., Hung, Y.P., Huang, L., Kim, D., Le, A., Yellen, G., Albeck, J.G., *et al.* (2014). Quantitative determinants of aerobic glycolysis identify flux through the enzyme GAPDH as a limiting step. Elife *3*, e03342.

Sonveaux, P., Végran, F., Schroeder, T., Wergin, M.C., Verrax, J., Rabbani, Z.N., De Saedeleer, C.J., Kennedy, K.M., Diepart, C., and Jordan, B.F. (2008). Targeting lactate-fueled respiration selectively kills hypoxic tumor cells in mice. The Journal of clinical investigation *118*, 3930-3942.

Stanley, W.C., Wisneski, J.A., Gertz, E.W., Neese, R.A., and Brooks, G.A. (1988). Glucose and lactate interrelations during moderate-intensity exercise in humans. Metabolism *37*, 850-858.

Witney, T.H., Kettunen, M.I., and Brindle, K.M. (2011). Kinetic modeling of hyperpolarized 13C label exchange between pyruvate and lactate in tumor cells. Journal of Biological Chemistry *286*, 24572-24580.

Zamboni, N., Fendt, S.-M., Rühl, M., and Sauer, U. (2009). 13 C-based metabolic flux analysis. Nature protocols *4*, 878.

Zhang, M., Qiu, Q., Li, Z., Sachdeva, M., Min, H., Cardona, D.M., DeLaney, T.F., Han, T., Ma, Y., Luo, L., *et al.* (2015). HIF-1 Alpha Regulates the Response of Primary Sarcomas to Radiation Therapy through a Cell Autonomous Mechanism. Radiation Research *183*, 594-609.

Figure 1

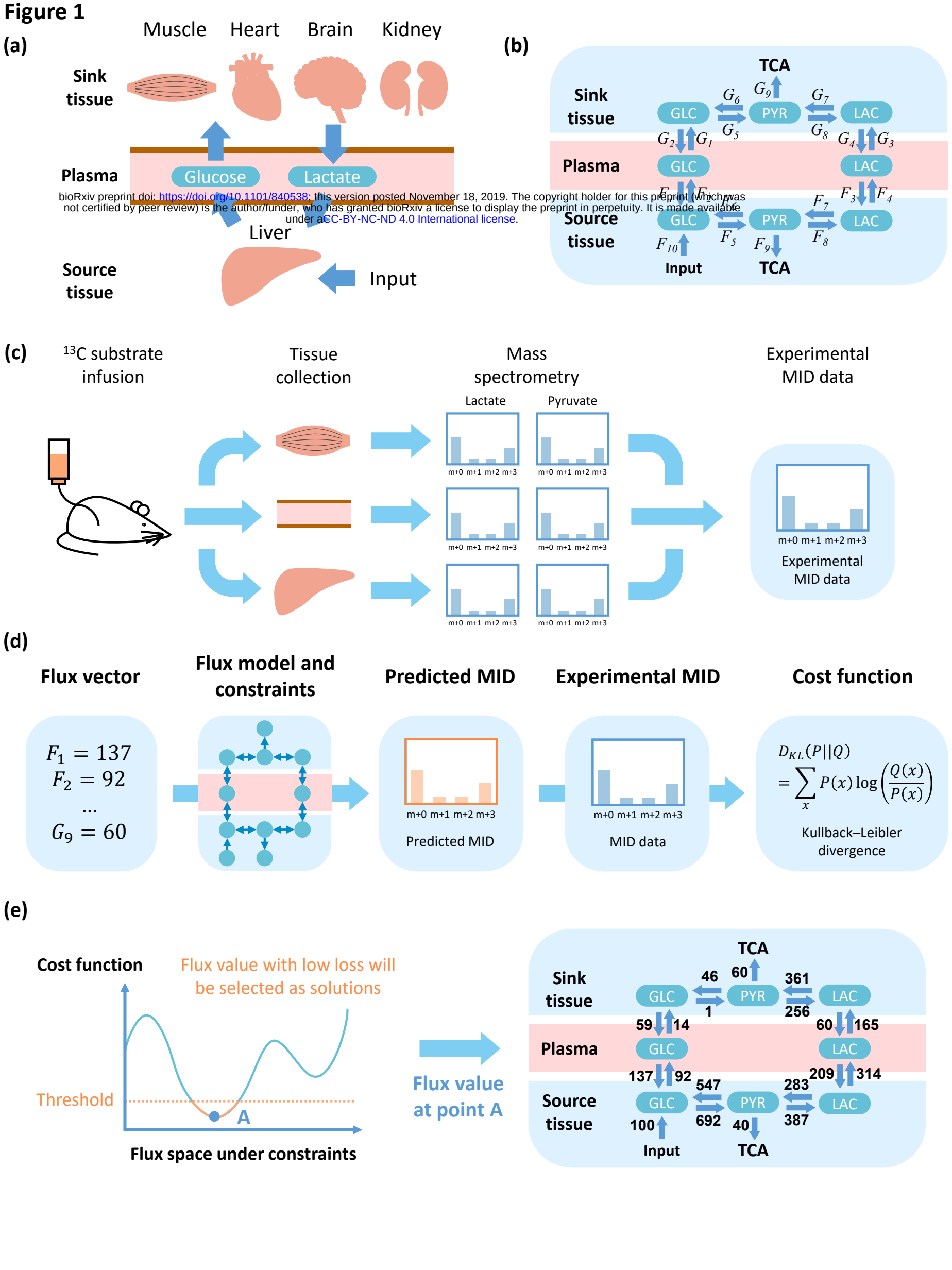

Figure 2

(a)

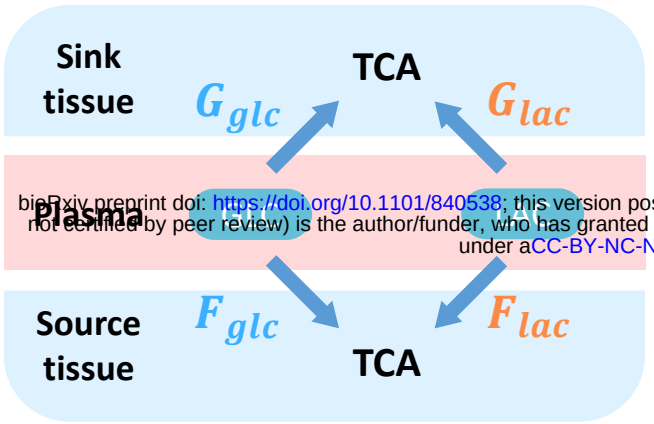

(b) Glucose contribution

TCA fluxes from glucose

$$R_{glc} = \frac{F_{glc} + G_{glc}}{F_{glc} + G_{glc} + F_{lac} + G_{lac}}$$

TCA fluxes from lactate

$$0 \le R_{glc} \le 1$$

$R_{glc} > 0.5$: Higher contribution from glucose

$R_{glc} < 0.5$: Higher contribution from lactate

(c)

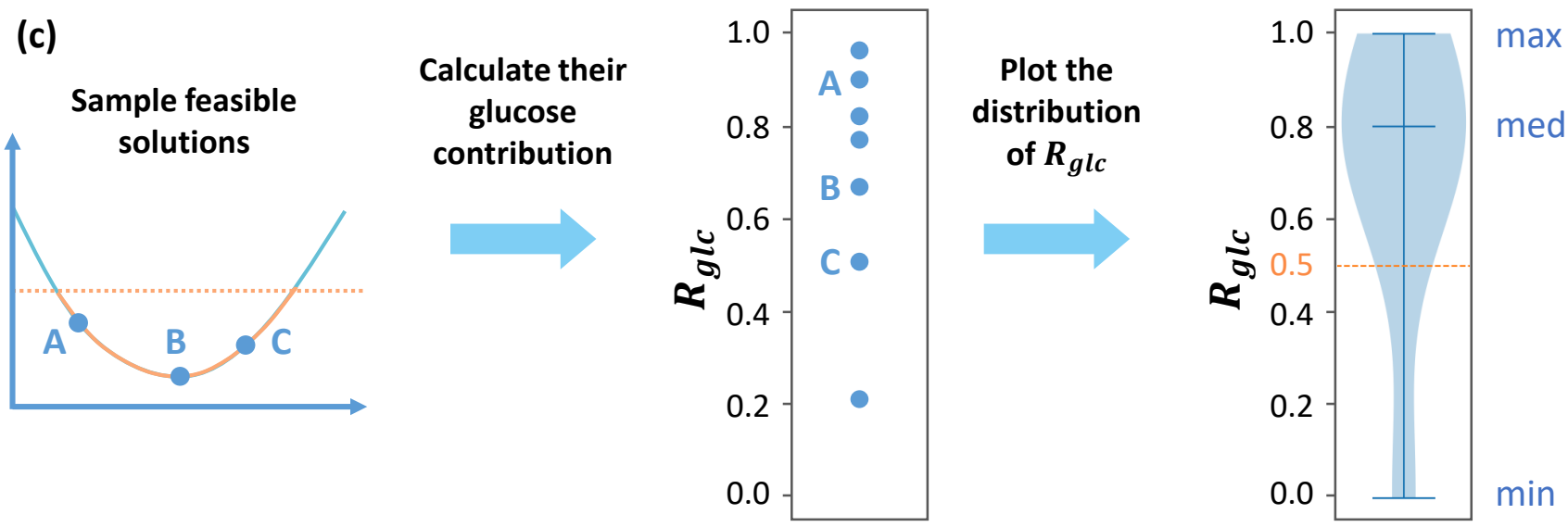

(d)

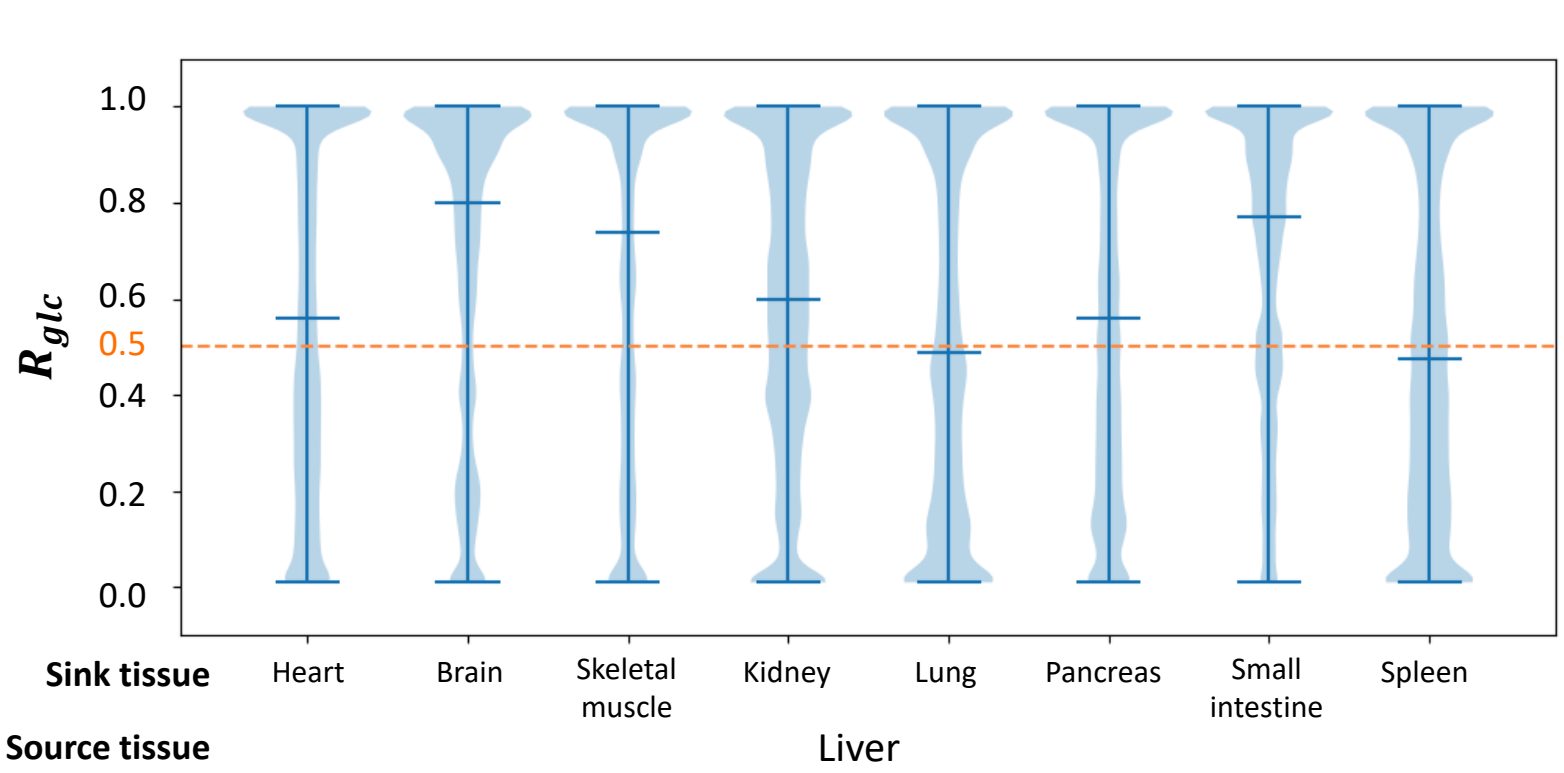

Figure S1

Experimental MID Predicted MID

Fitting result when value of objective function equals to **0.1**

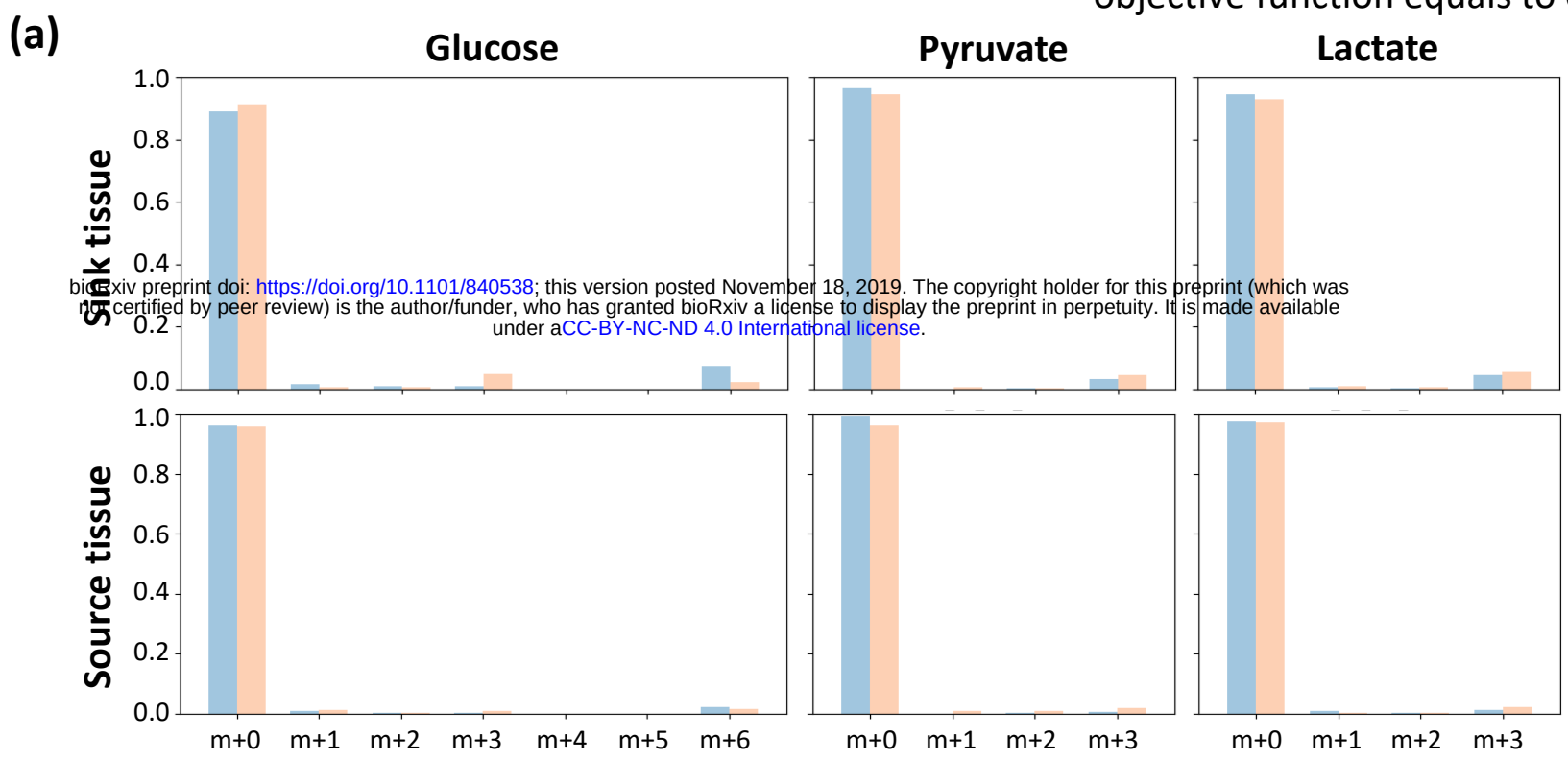

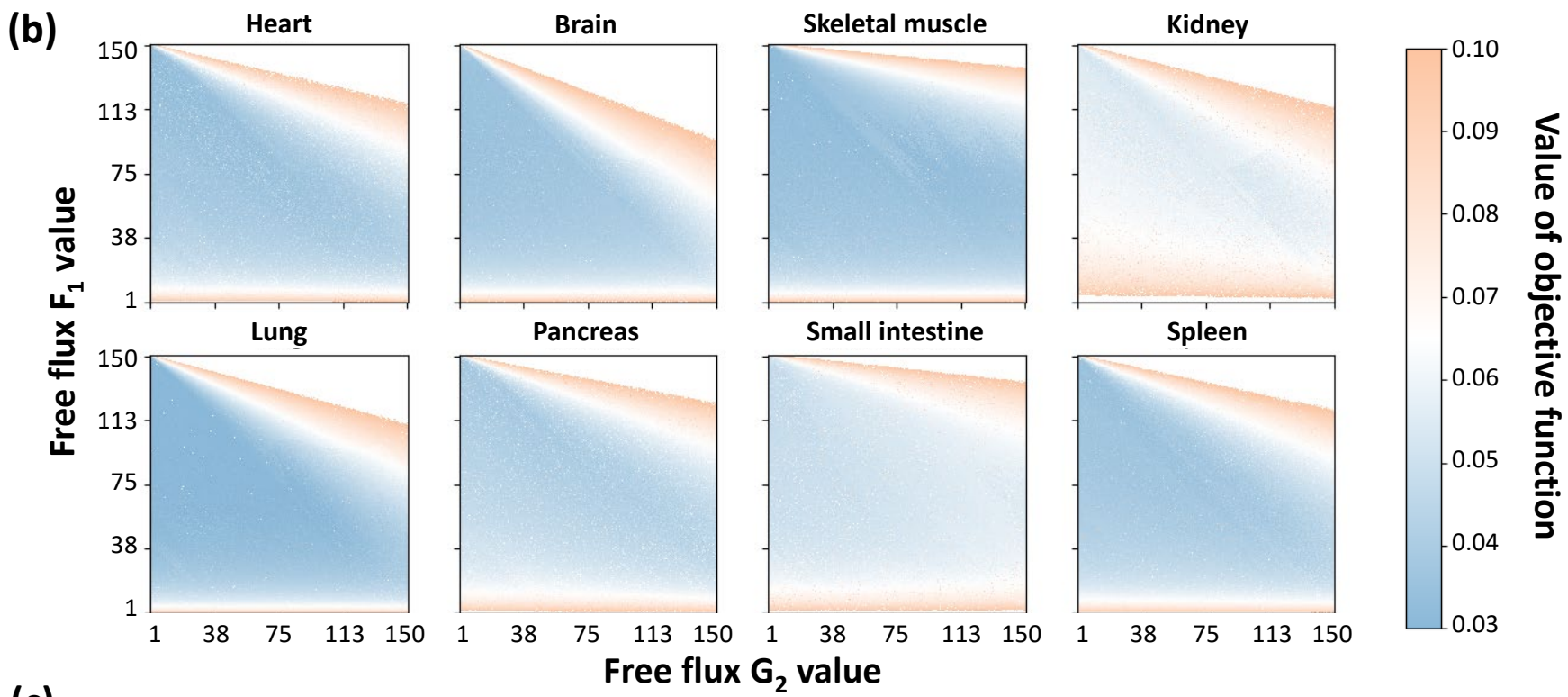

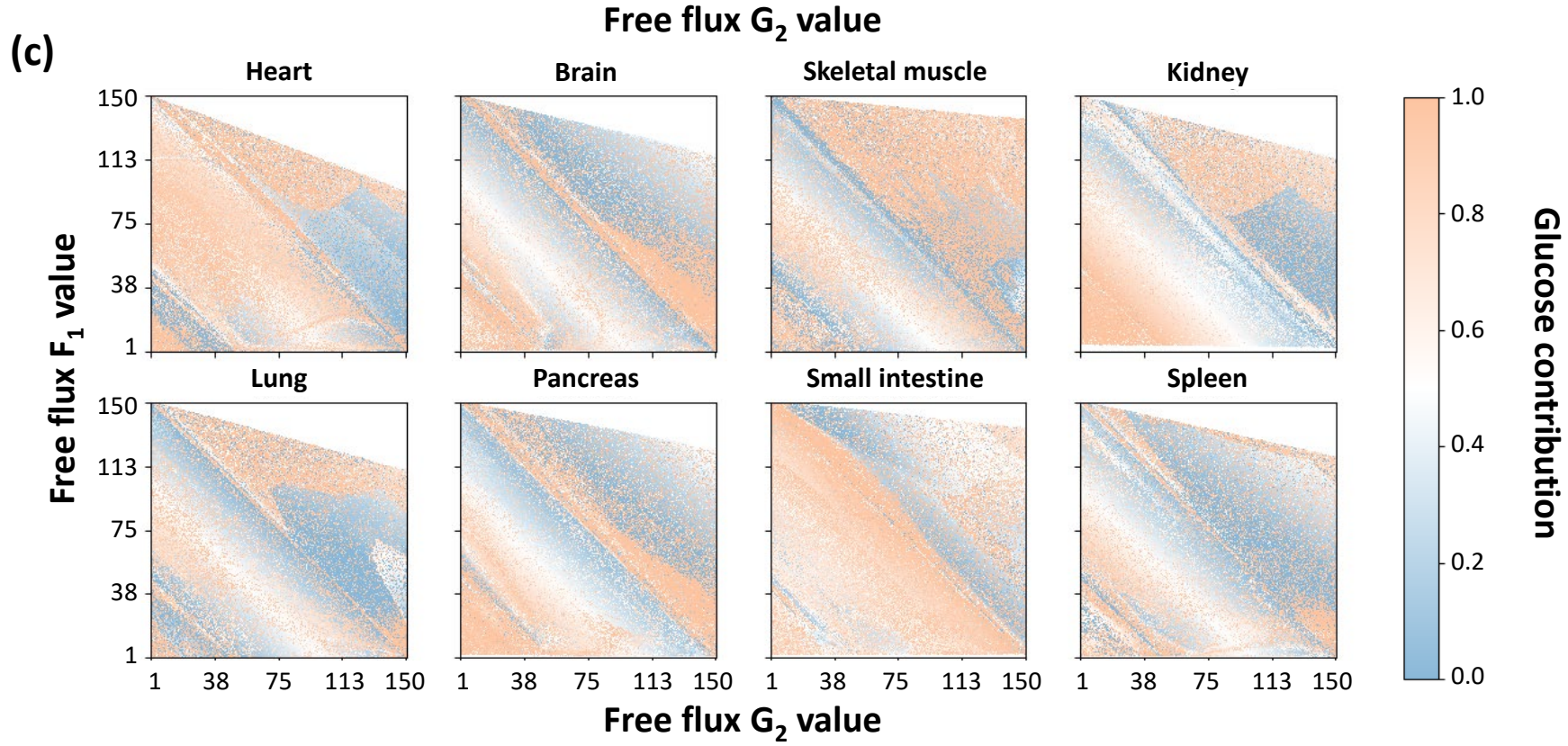

Figure S2

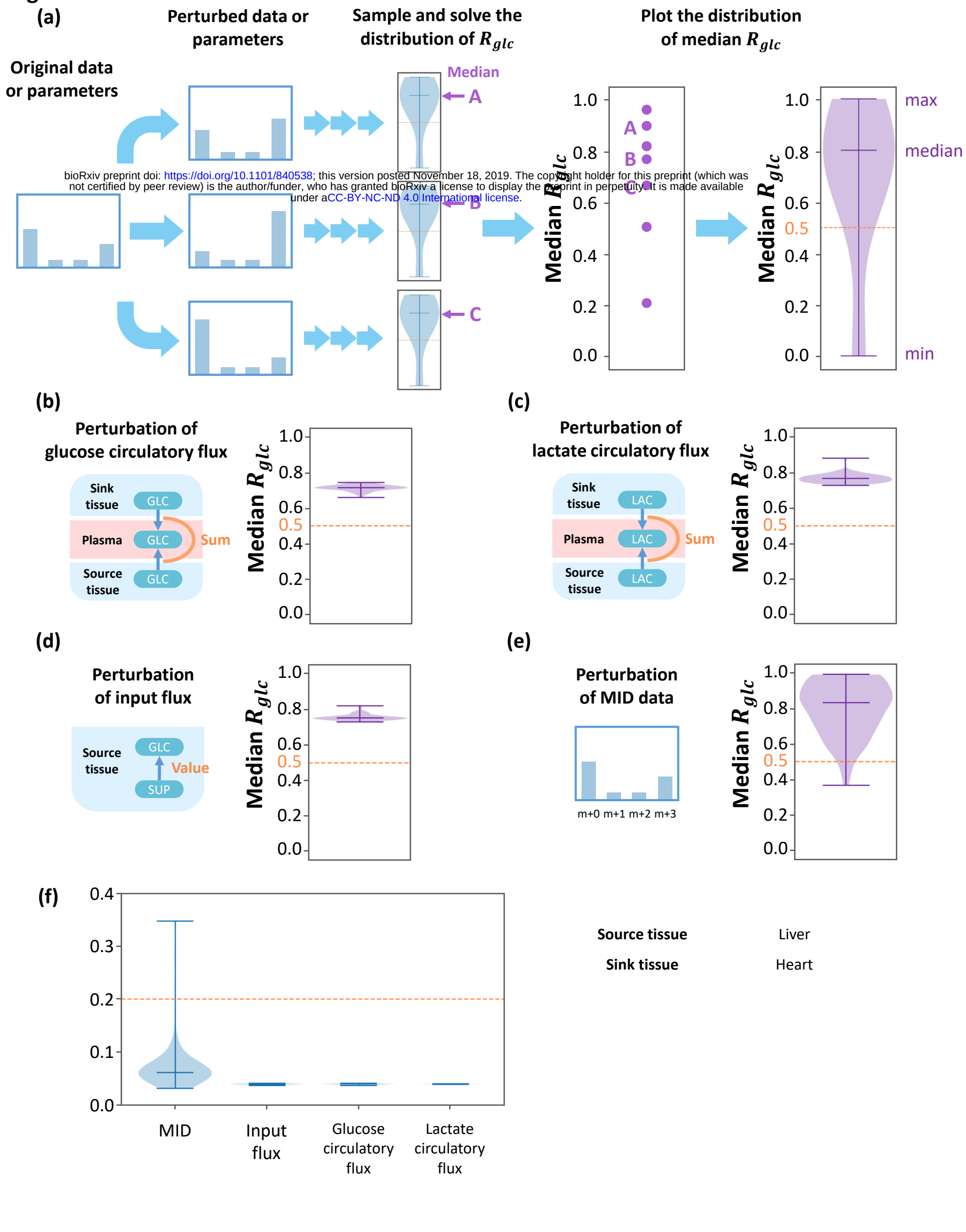

Figure 3

(a) MID data

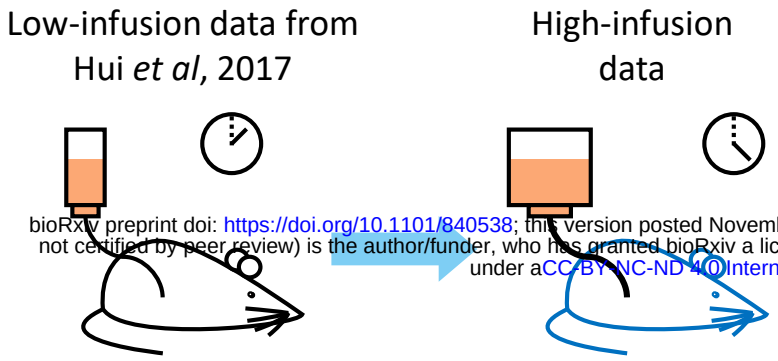

(b)

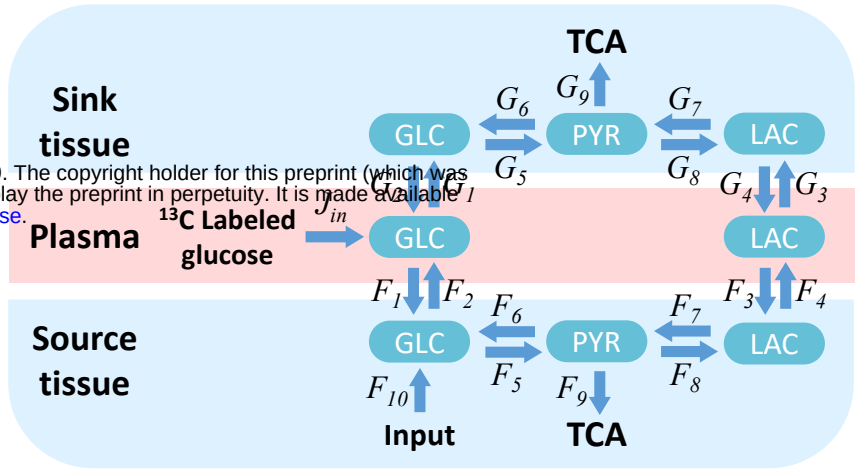

(c)

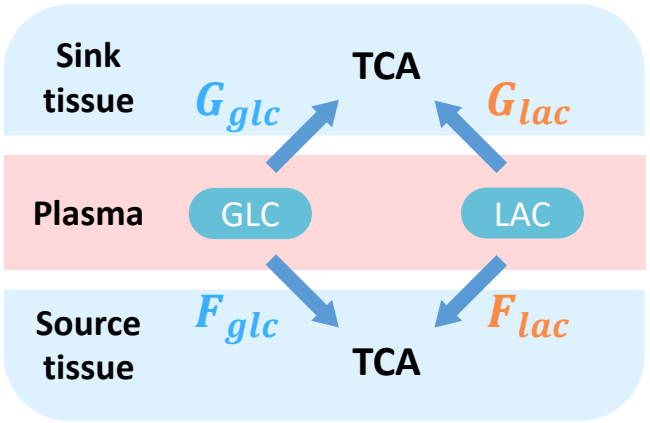

(d)

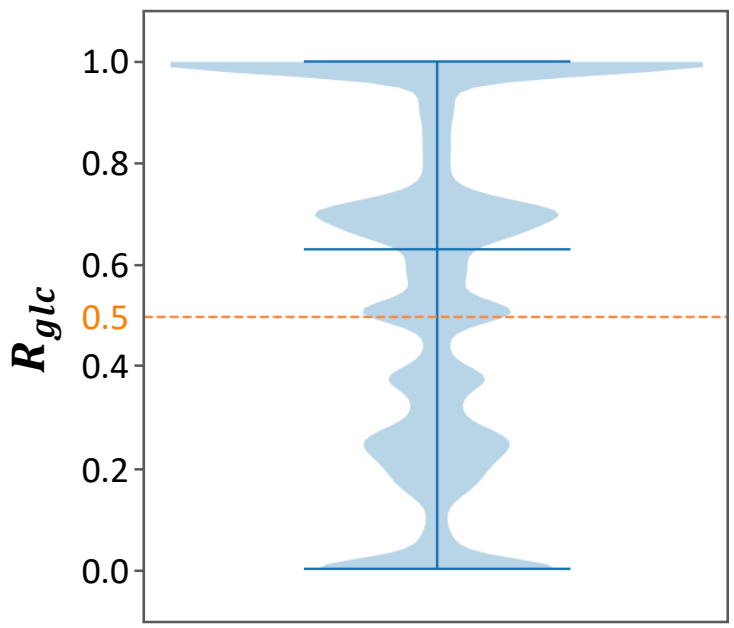

Source tissue	Liver
Sink tissue	Skeletal muscle
Data	High-infusion data

Glucose contribution

$$R_{glc} = \frac{\text{TCA fluxes from glucose}}{\text{TCA fluxes from glucose} + \text{TCA fluxes from lactate}} = \frac{F_{glc} + G_{glc}}{F_{glc} + G_{glc} + F_{lac} + G_{lac}}$$

Figure S3

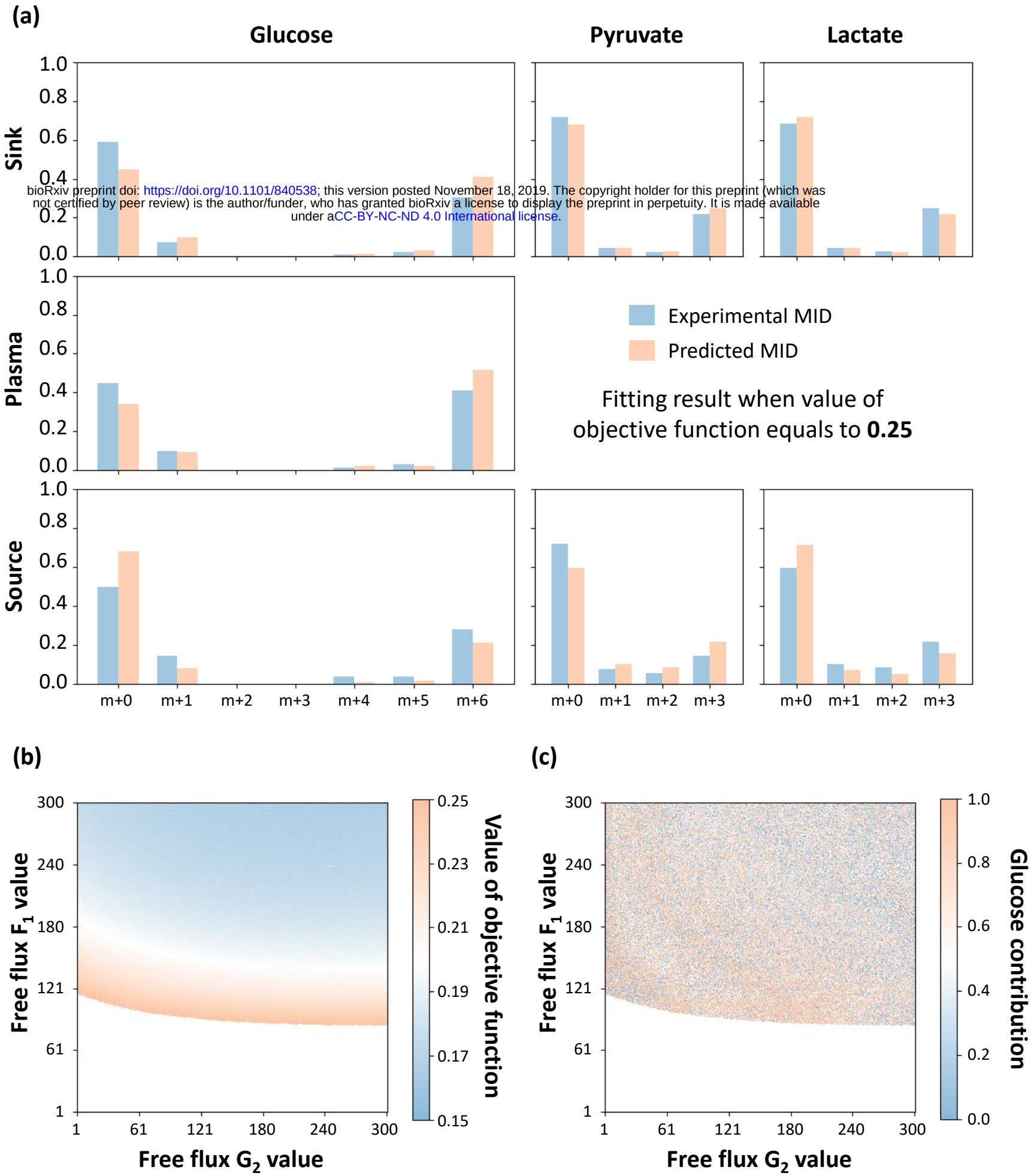

Figure 4

(a) Tissue type in model

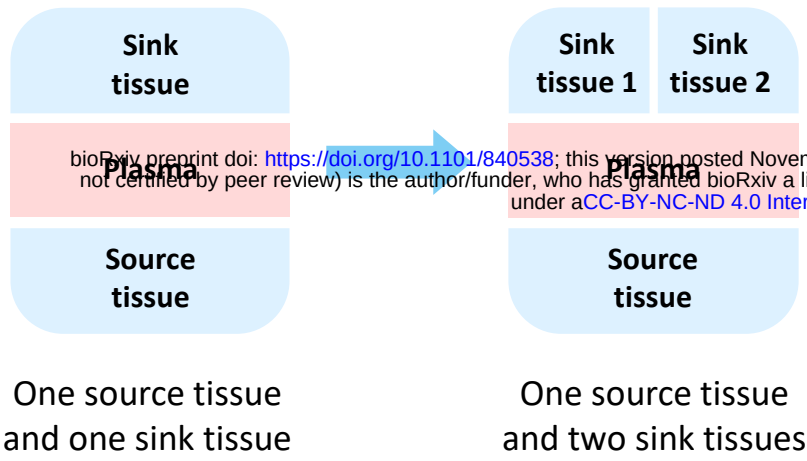

One source tissue and one sink tissue

One source tissue and two sink tissues

(b)

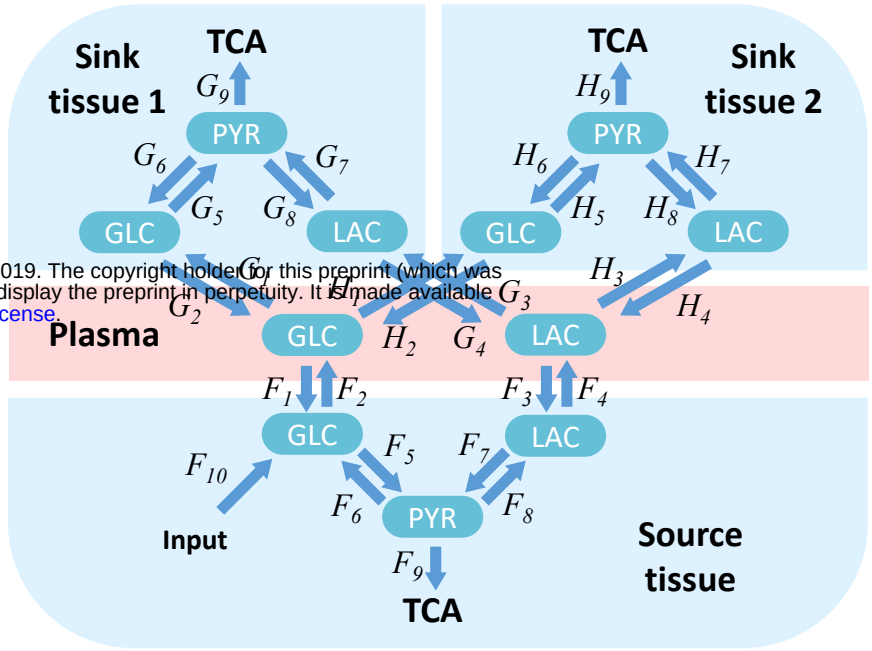

(c)

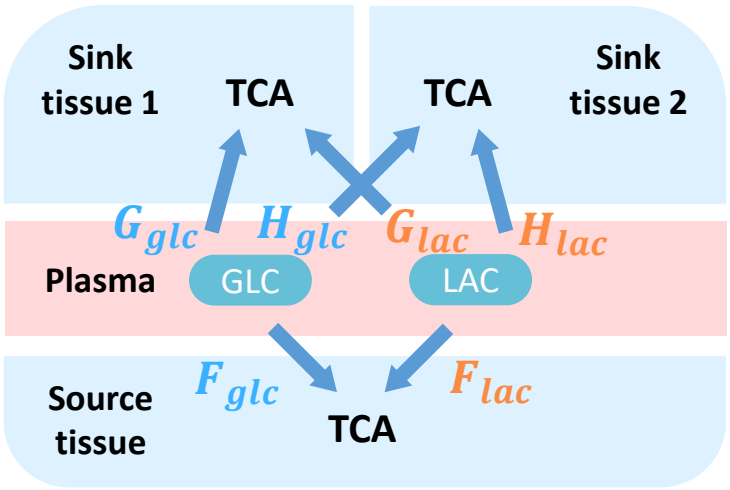

(d)

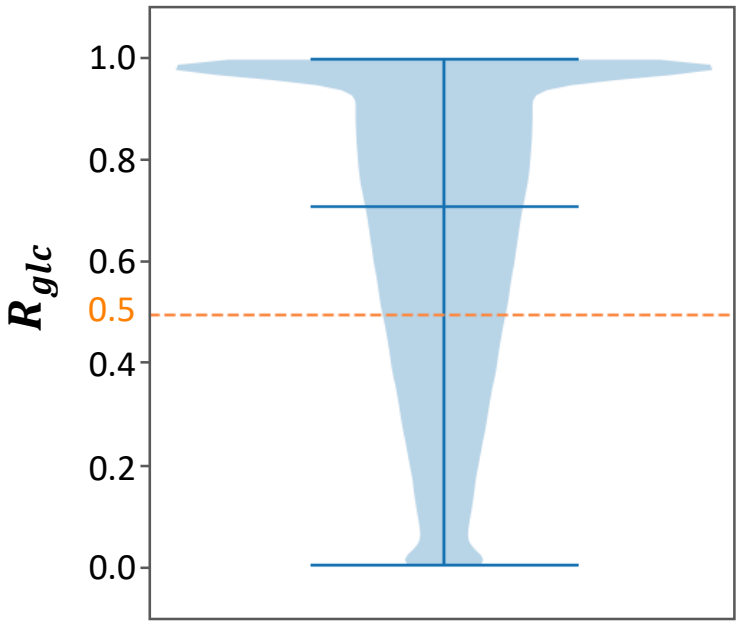

Source tissue	Liver
Sink tissue 1	Heart
Sink tissue 2	Skeletal muscle
Data	Low-infusion data

Glucose contribution

TCA fluxes from glucose

$$R_{glc} = \frac{F_{glc} + G_{glc} + H_{glc}}{F_{glc} + G_{glc} + H_{glc} + F_{lac} + G_{lac} + H_{lac}}$$

TCA fluxes from lactate

Figure S4

(a)

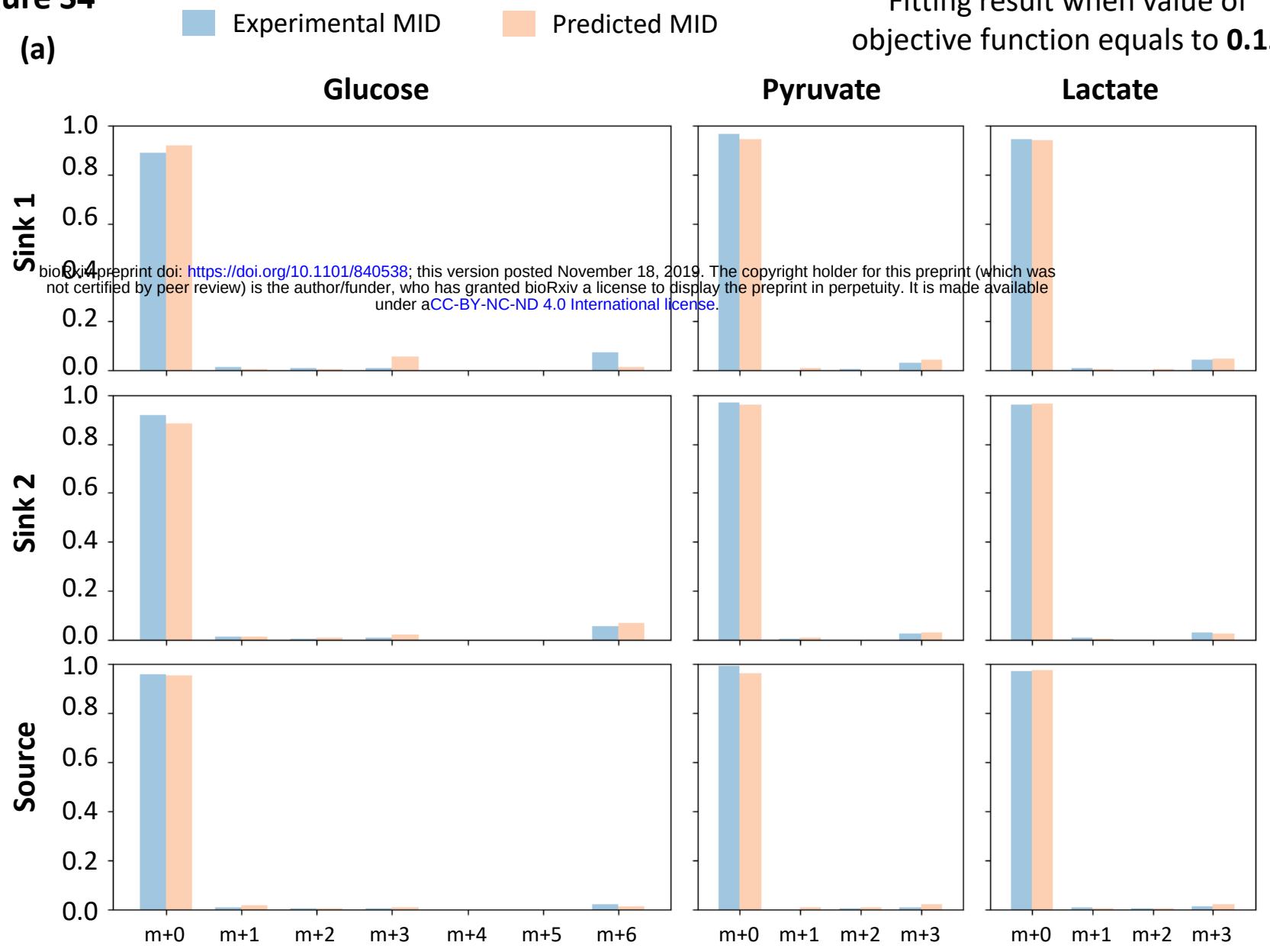

(b)

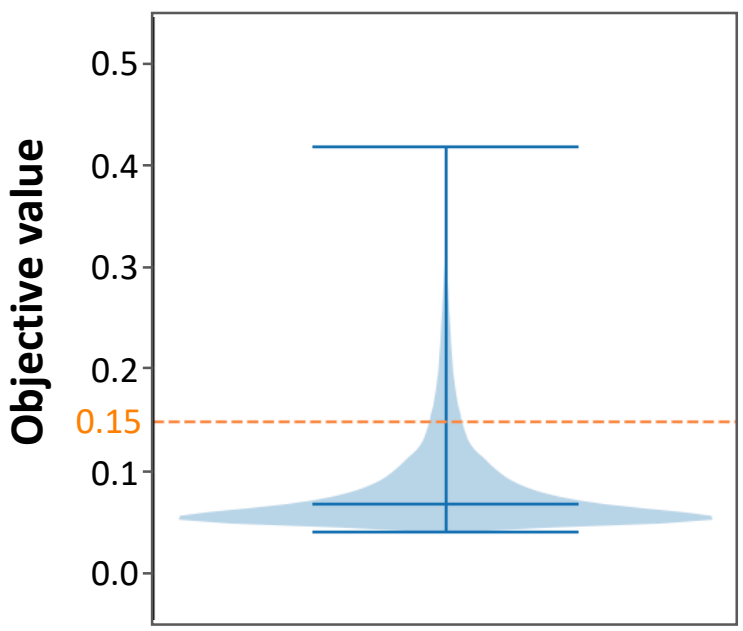

Figure 5

(a) Circulating metabolites in model

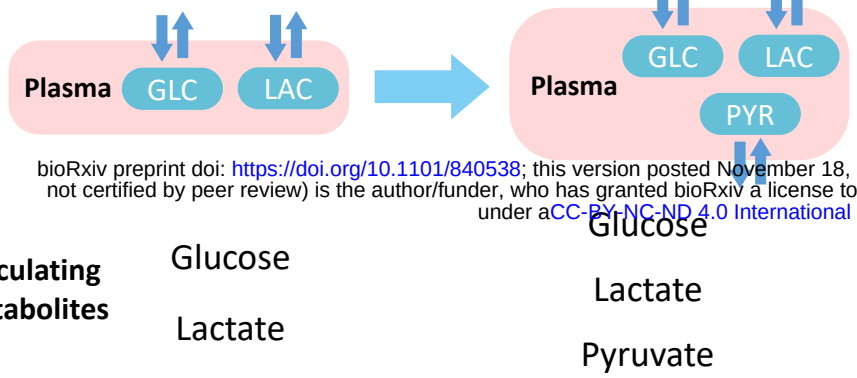

Circulating metabolites		
	Glucose	Glucose
	Lactate	Lactate
		Pyruvate

(b)

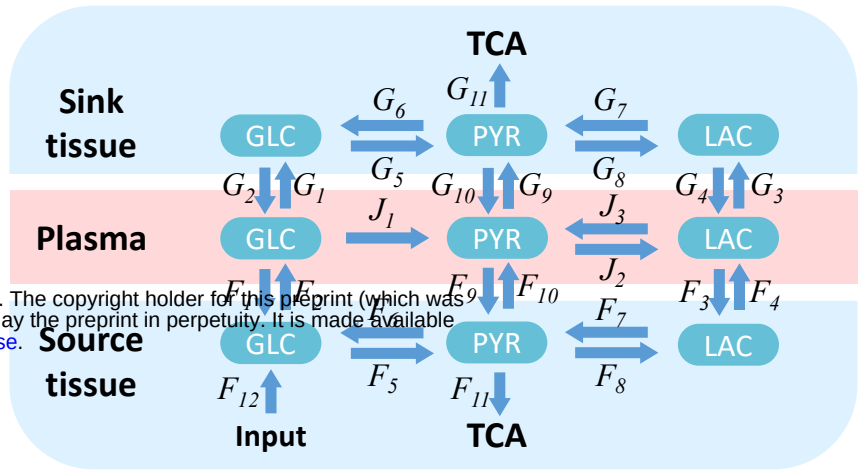

(c)

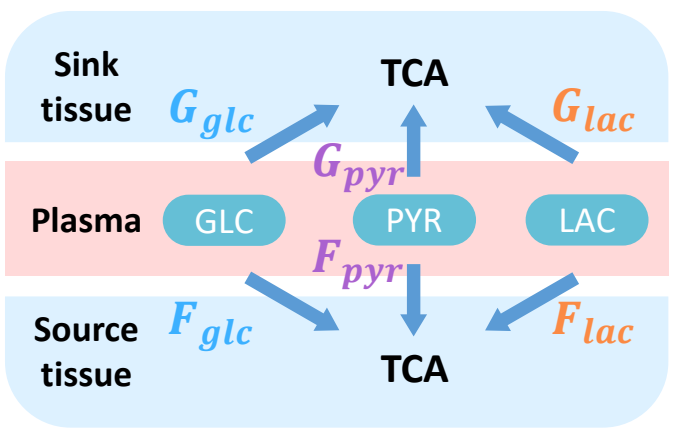

Glucose contribution

$$R_{glc} = \frac{F_{glc} + G_{glc}}{F_{glc} + G_{glc} + F_{lac} + G_{lac} + F_{pyr} + G_{pyr}}$$

TCA fluxes from glucose

TCA fluxes from lactate

TCA fluxes from circulating pyruvate

Lactate contribution

$$R_{lac} = \frac{F_{lac} + G_{lac}}{F_{glc} + G_{glc} + F_{lac} + G_{lac} + F_{pyr} + G_{pyr}}$$

Pyruvate contribution

$$R_{pyr} = \frac{F_{pyr} + G_{pyr}}{F_{glc} + G_{glc} + F_{lac} + G_{lac} + F_{pyr} + G_{pyr}}$$

(d)

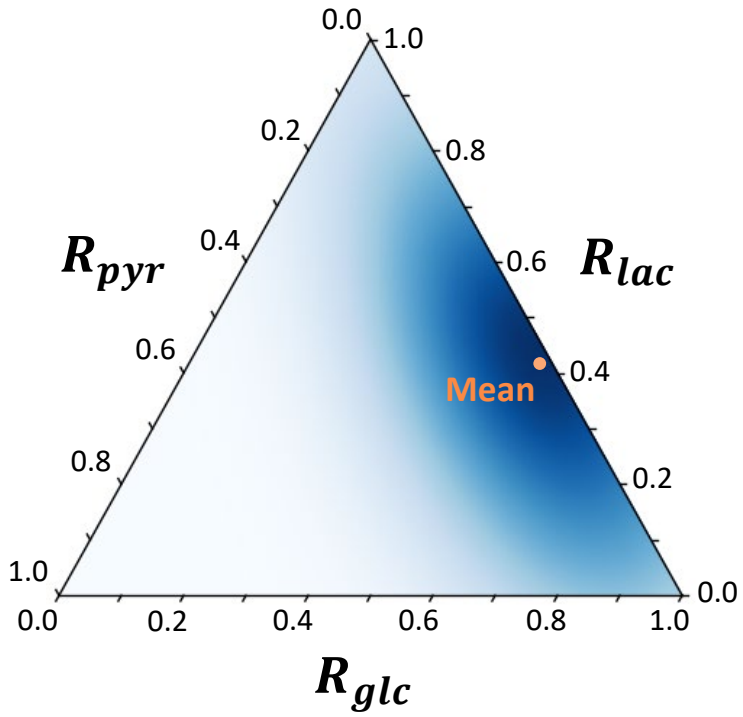

Source tissue	Liver
Sink tissue	Heart
Data	Low-infusion data

(e)

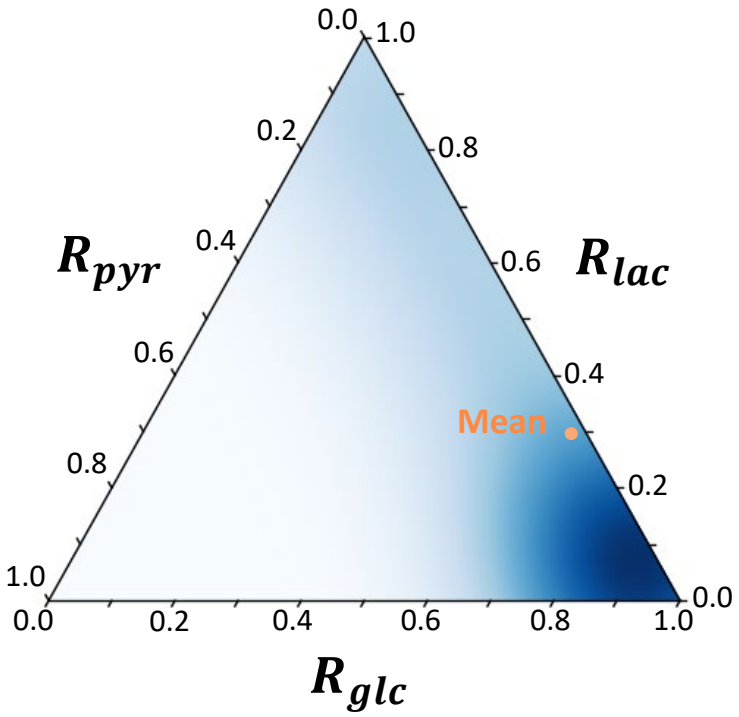

Source tissue	Liver
Sink tissue	Skeletal muscle
Data	High-infusion data

Figure S5

Experimental MID

Predicted MID

(a)

Fitting result when value of objective function equals to **0.15**

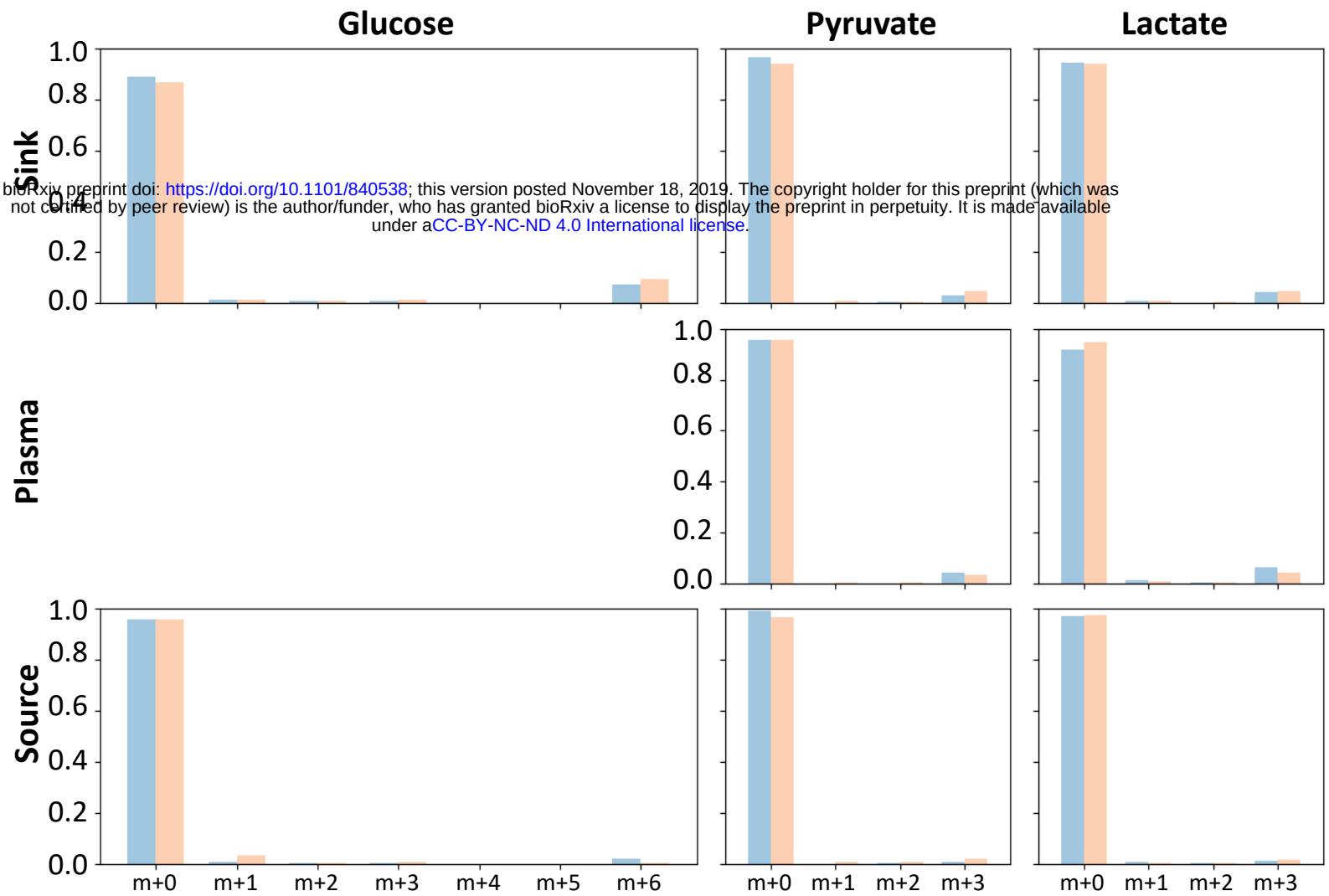

(b)

Fitting result when value of objective function equals to **0.25**

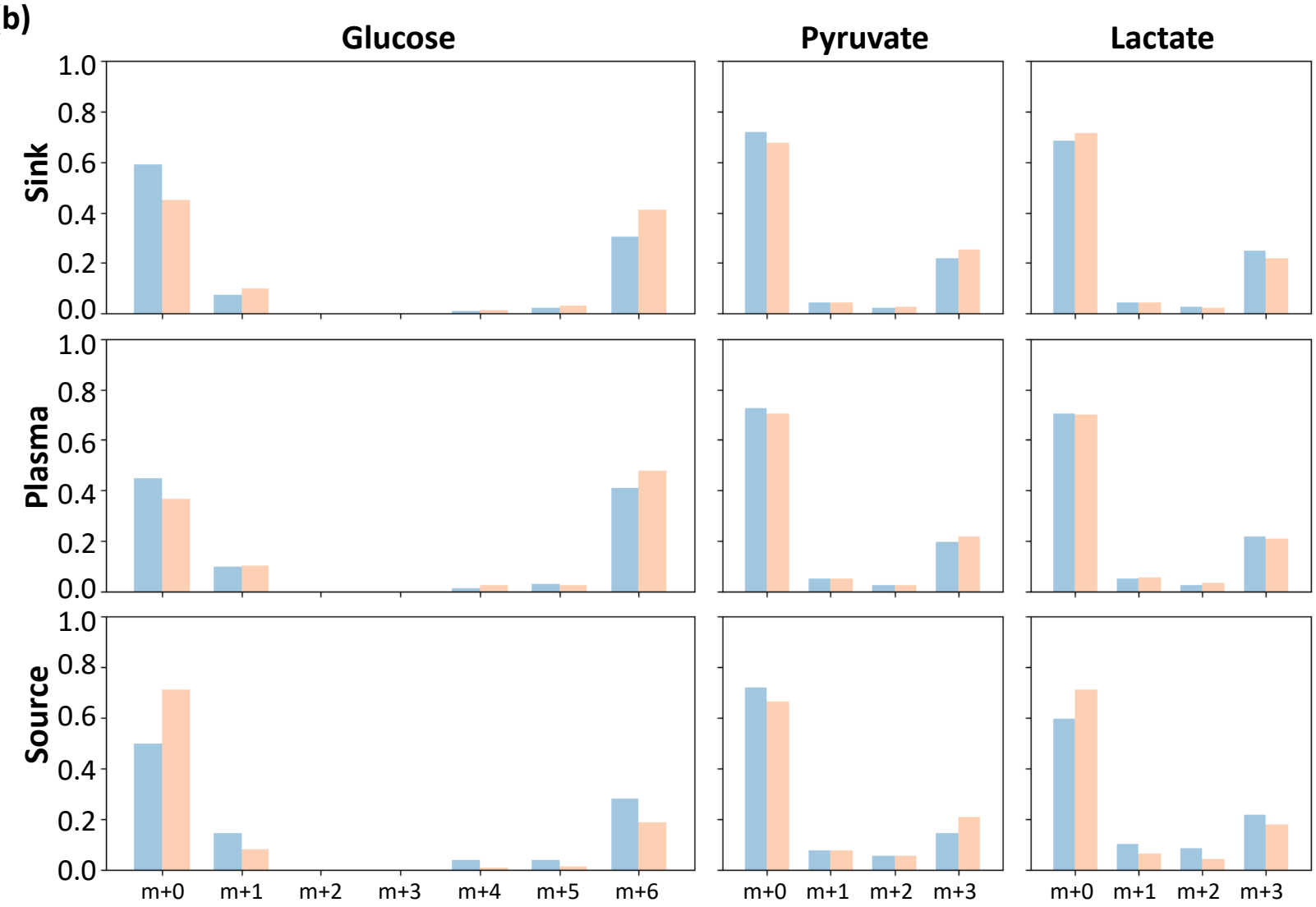

Figure S6

(a)

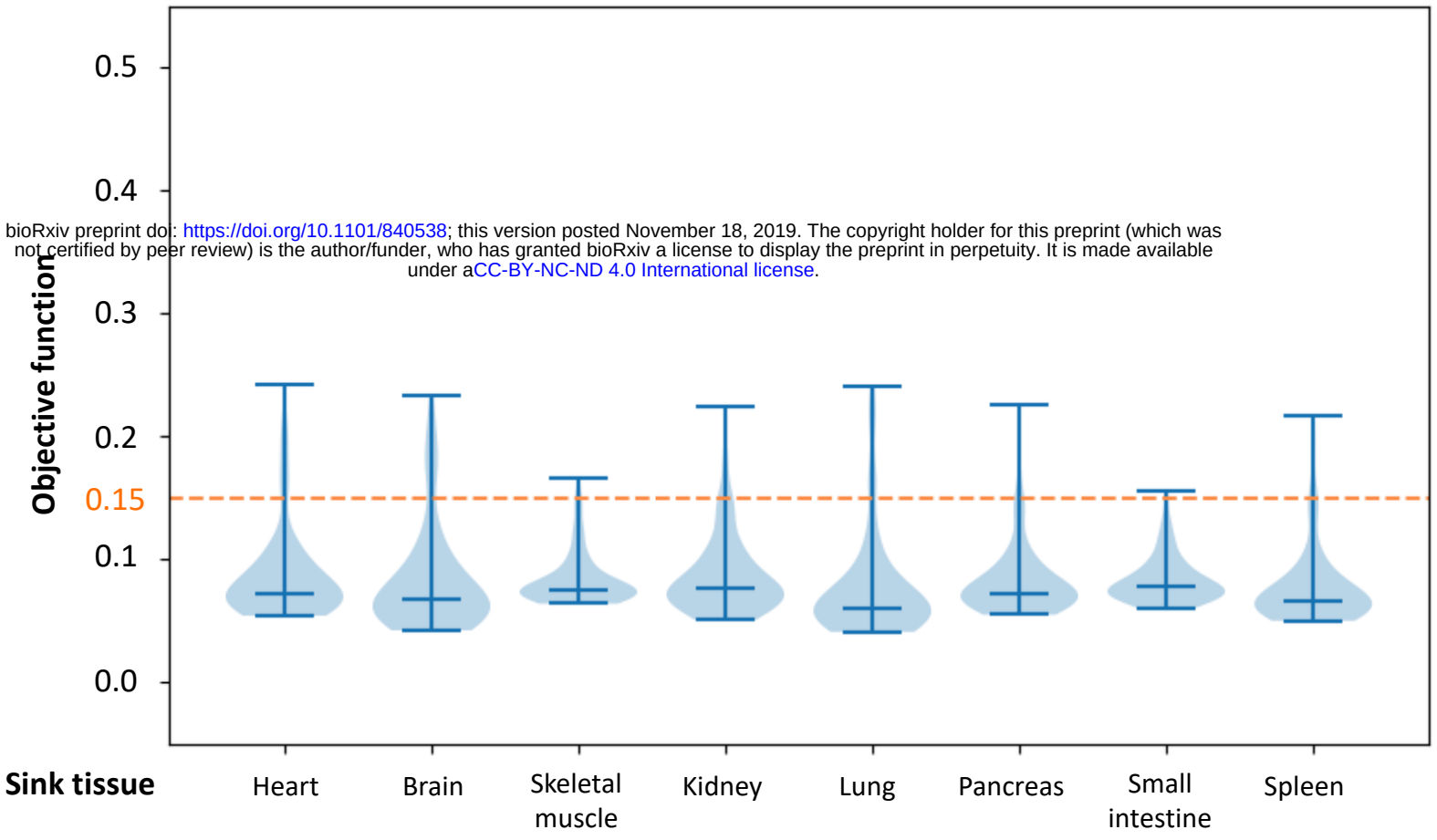

(b)